

# Method for Automated Parametric Studies and Evaluation Using the Example of an Aerosol-on-Demand Jet-Printhead

Hanna Pfannenstiel, Martin Ungerer<sup>a</sup> and Ingo Sieber<sup>b</sup>

*Institute for Automation and Applied Informatics, KIT, Hermann-von-Helmholtz-Platz 1, 76344 Eggenstein-Leopoldshafen, Germany*


**Keywords:** Computational Fluid Dynamics, Modelling, Simulation, Model Reduction, Additive Manufacturing, Aerosol-on-Demand.


**Abstract:** In this paper, we present a method for the automated determination of aerosol jet parameters for the Aerosol-on-Demand (AoD) jet-printhead. A critical aspect in the simulation of our computational fluid dynamics (CFD) model is the simulation time due to the high model complexity in combination with a large number of individual elements. This, together with the problem of determining the focal point through measurements on our laboratory setup, leads to our approach of model reduction as the basis for an automated determination of the aerosol jet parameters, which is shown using the example of determining the focal position and focal width. Starting from a fluid dynamic model, we create a reduced model by separating the variables, with which we can predict aerosol jet parameters. The method presented here is validated by CFD simulations of an aerosol spray with a mass of individual droplets are varied according to a Rosin-Rammler distribution.

## 1 INTRODUCTION

The functional printing of nanomaterials offers new possibilities for the realization of electronic circuits (Baby et al., 2020; Gengenbach et al., 2018; Cui, 2016; Suganuma, 2014; Choi et al., 2015), e.g. on flexible substrates and 3D components, for which conventional lithography-based subtractive manufacturing processes are not suitable (IDTechEx Ltd., 2022). The printing of functional inks also opens up new possibilities for the realization of special physical, optical or chemical properties (Sirringhaus and Shimoda, 2003; Sieber et al., 2020a,b; Magdassi, 2010). In general, digital printing processes for functional printing can be categorized as Drop-on-Demand (DoD) inkjet or aerosol jet printing processes. The DoD inkjet printing process in particular has established itself in the additive manufacturing of functional structures. However, it has the inherent disadvantage that it requires a constant distance between the nozzle and substrate in the range of approx. 0.3 mm to 1 mm in order to achieve high print quality. This process requirement makes the printing of 3D structures very complex or impossible. The

aerosol jet printing process offers an alternative for functional printing in terms of higher resolution and the possibility of printing on 3D structures. The basis of this printing process is the atomization of the ink into a fine spray and the subsequent hydrodynamic focusing by means of a sheath gas flow and nozzle geometry. The result is an aerosol jet that is collimated over a range of several millimeters, i.e. the jet width does not change in this range. This collimation range makes it possible for the printed line width to be independent of the distance between the nozzle outlet and the substrate. This enables the aerosol jet printing process to print on uneven surfaces and surfaces of any shape. The aerosol jet printing process is currently realized as a continuous printing process (Optomec Inc., 2024; IDS Inc., 2024), which requires a physical interruption of the jet to print discontinuous structures. A new principle for an Aerosol-on-Demand (AoD) jet-printhead is being developed at our institute (Ungerer et al., 2023c), which basically enables high-frequency switching on and off of the aerosol generation with an established sheath gas flow and thus enables on-demand printing (Sieber et al., 2022). This is achieved by atomizing tiny amounts of functional ink directly in the printhead. The resulting compact system design also enables printing in all spatial directions and a widely adjustable distance

<sup>a</sup>  <https://orcid.org/0009-0000-4026-6338>

<sup>b</sup>  <https://orcid.org/0000-0003-2811-7852>

between the nozzle and substrate (Ungerer, 2020). Based on computational fluid dynamics (CFD) simulations, the design-for-manufacturing of a laboratory setup was created and implemented (Ungerer et al., 2022, 2023a). The CFD simulations were used to mutually evaluate different nozzle geometries (Ungerer et al., 2023b) and to determine tolerance influences in the position of the atomizer unit. The CFD simulations are very complex to calculate and require many hours to a few days for the calculation (the CFD simulations are carried out on a workstation equipped with AMD Ryzen Threadripper 3970X processor with 32 cores, 64 threads @ 3.7GHz, 128 GB RAM, and an Nvidia Titan RTX graphics processor with 24GB which is available at our institute. In order to allow other processes to still take place on the workstation, only 28 cores are utilized in the simulations of this paper.). In addition, when measuring the aerosol jet on the test setup, we realized that it is not possible to determine the jet width and the location of the focus position with our measurement equipment.

The contribution that we address in this paper is the automated determination of the focal position as a function of the droplet mass or its emission angle during aerosol generation on the basis of predictions made using a reduced model. The model reduction procedure is based on the separation of the mass and emission angle variables.

This paper is organized as follows: Section 2 describes the laboratory setup of the AoD printhead, Section 3 presents the CFD model and motivates the model reduction, which is used to determine the focal position of the droplets. Section 4 is dedicated to analyzing the derived method in comparison with the simulation of an aerosol spray with a mass distribution described by a Rosin-Rammler distribution. Section 5 deals with the discussion of the results and section 6 will close the paper with conclusions.

## 2 THE AoD SETUP

The AoD jet-printhead is shown schematically in Figure 1 and comprises an atomizer unit that generates the aerosol on demand and directly inside the printhead, an antechamber with four inlets for the sheath gas equidistantly distributed around the circumference of the printhead, a mixing chamber and a nozzle. The antechamber is designed to ensure a homogeneous annular sheath gas flow inside the mixing chamber of the printhead where the aerosol is ejected from the atomizer unit and to directly focus the aerosol in combination with the inner contour of the mixing chamber and the nozzle. The nozzle of the

printhead is manufactured in two parts (Ungerer et al., 2023a).

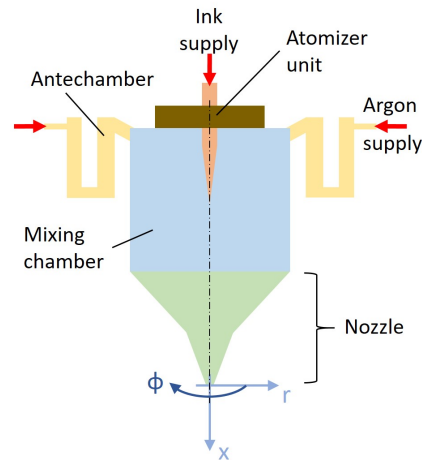


Figure 1: Schematic of the AoD jet-printhead.

The fabricated laboratory prototype of the developed AoD jet-printhead is integrated into a laboratory test setup in order to characterize the generated aerosol jet after the nozzle exit (Sieber et al., 2022).

The laboratory test setup, consisting of an ink supply, a sheath gas supply, the printhead with a function generator and an optical observation equipment, is schematically depicted in Figure 2.

The ink supply comprises an ink reservoir, a time-pressure dispenser that is used as open-loop control of the pressure inside the ink reservoir and a mobile air compressor acting as compressed air supply for the dispenser. The sheath gas supply is composed of an Argon gas cylinder with a pressure regulator, a mass flow controller and manifolds. The ink supply is connected to the atomizer unit of the printhead. The actuator of the atomizer unit is connected to the frequency generator. Water is used as test fluid. The sheath gas supply is connected to the four inlets of the antechamber of the printhead. The aerosol jet after nozzle exit is studied by means of a Keyence VHX-7020 digital camera with a Keyence VH-Z20R microscope zoom lens and a 20 W Tapfer 5004LTF LED light, inclined by  $45^\circ$  to the camera's optical axis.

Figure 3 shows images of the aerosol jet after the nozzle exit. As can be seen from Figure 3 a), the aerosol jet is collimated over a length of about 60 mm after the nozzle exit. Images taken with higher magnification (Figures 3 b) and c)) reveal that it is almost impossible to precisely measure the real diameter of the aerosol jet and to determine the focal position with the presented setup, in particular, as individual droplets outside the actual, clearly visible beam are hardly to be detected.

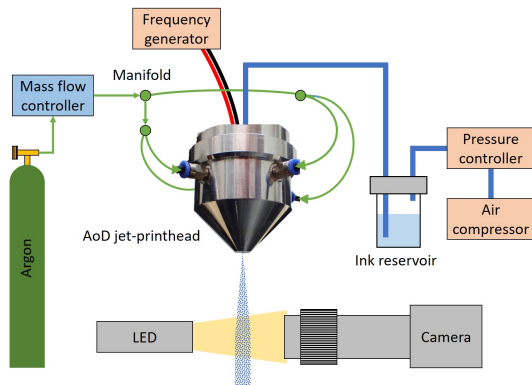


Figure 2: Schematic of the optimized laboratory setup.

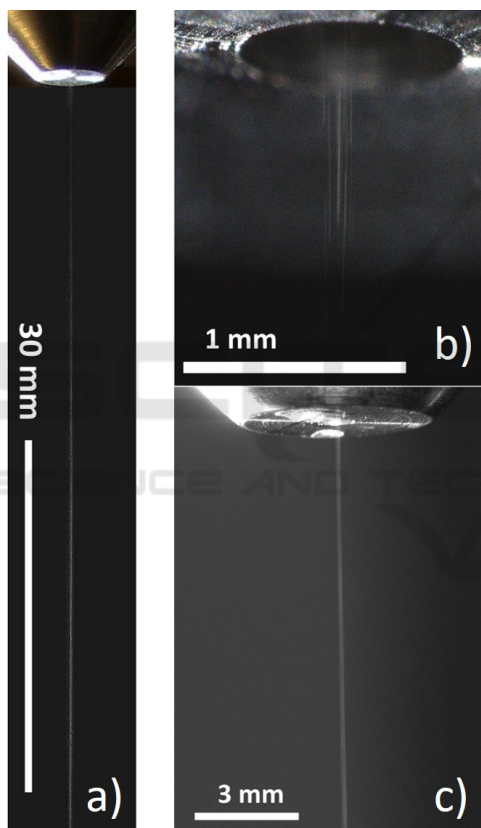


Figure 3: Microscope images showing a) the collimation length, b) the nozzle orifice and c) the focused aerosol jet at planned working distance after nozzle exit).

### 3 MODELING

#### 3.1 The CFD Model

As previously mentioned the AoD Printer is a use case that is very difficult to do physical measurements on.

Therefore a Computer Fluid Dynamics (CFD) model has been created to gain more information about the flow regime that is important to the functionality of the device. CFD is an established technology which calculates flow regimes based on the Navier-Stokes equations. The CFD software used in this paper is Ansys Fluent 2023 R2. In most situations a Direct Numerical Simulation (DNS) through the Navier-Stokes equations is too computationally expensive if turbulence phenomena on a multitude of scales should be represented. Therefore averaging terms and turbulence models are necessary to simulate the phenomena. For computationally economic reasons the Reynolds-Averaged Navier-Stokes (RANS) in combination with the  $k-\omega$ -SST turbulence model was chosen as they provide the required accuracy for most engineering applications while not increasing the computational time significantly (Sieber et al., 2022). Interested readers can find more detailed information about the RANS and  $k-\omega$  models in Wilcox (2006) and Menter (1994).

The CFD model features the geometry of the printhead starting at the inlet channels to the homogenization chamber as well as an area that spans 26 mm past the nozzle exit to simulate the free jet.

The mesh in CFD simulations greatly influences the quality of the result. Areas with high gradients need a fine mesh for the gradients to not get lost in the averaging over an element. Additionally, structured meshes which are aligned with the direction of the flow improve numerical diffusion (Ungerer et al., 2022). Unstructured meshes on the other hand offer a simpler meshing process and they require less control to ensure that they are set up properly. As the area of the free jet is of great interest a structured, hexahedral mesh will be used. The mesh of the free jet features elements with smaller length near the nozzle exit and longer cells towards the end as can be seen in Figure 5. Inside the printhead the center is meshed structurally with finer cell resolution. In the mixing chamber an unstructured tetrahedral mesh is generated as the flow in those domains is less important and computational resources can be saved. The generated mesh for the inside of the printhead can be seen in Figure 4.

As the Euler-Lagrange model used to track the discrete phase involves particles the cell size must be large enough for a particle to be entirely contained in a single cell. Ungerer et al. (2023a) measured a droplet size of up to  $20\ \mu\text{m}$  at the capillary exit. A previous independence study dealt with the level of detail in the mesh and found a mesh with 2.1 million elements to be sufficiently accurate with any increase in the mesh precision not necessarily resulting in a

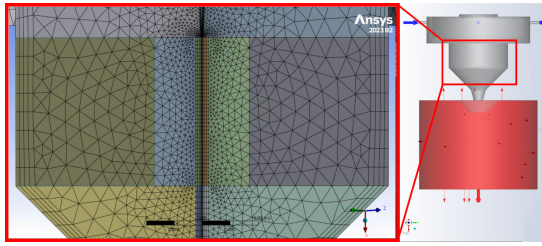


Figure 4: The mesh of the mixing chamber.

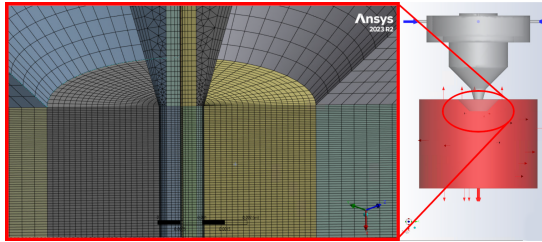


Figure 5: The mesh at the beginning of the free jet area.

worthwhile trade-off of improved accuracy over calculation time (Ungerer et al., 2023d). The minimum element size in this mesh is  $33\ \mu\text{m}$  which fulfills the condition set by tracking of the discrete phase.

As it is the final goal, a stationary solution is evaluated in the CFD simulation where the sheath gas has a fully developed flow. From that follows the assumption that the entire printhead is completely filled with the sheath gas Argon while the free jet area is predominantly air. While gases have similar densities and viscosities in absolute terms comparing their material properties relatively shows a bigger difference. In order to properly model the interaction in the free jet as the two gases mix a multiphase model is utilized. Ansys provides multiple multiphase models that vary in their use case and complexity. For this application the Volume-of-Fluid (VoF) model is chosen. It introduces the volume fraction as an additional variable to solve for each cell in the continuous equations. The volume fraction is calculated according to Equation 1 (ANSYS, Inc., 2023a) where  $q$  is the index of the phase,  $\dot{m}_{pq}$  is the mass transport between phases and  $S_{\alpha_q}$  is a user-definable mass source. In our model we use its default value zero.

$$\frac{1}{\rho_q} \left[ \frac{\partial}{\partial t} (\alpha_q \rho_q) + \nabla \cdot (\alpha_q \rho_q \vec{v}_q) \right] = S_{\alpha_q} + \sum_{p=1}^n (\dot{m}_{pq} - \dot{m}_{qp}) \quad (1)$$

All other material properties such as viscosity and density are derived by linear blending of the values of each individual material through its volume fraction. The interfacial areas of the phases are afterwards reconstructed from the volume fractions. As air and argon don't form a sharp interface a dispersed modeling was chosen to reflect the area of mixture.

### 3.2 Determining the Focal Point

The focal point of the aerosol jet is the cross section in which the aerosol covers the smallest area. The coordinate system used throughout this paper can be seen in Figure 1: Cylindrical coordinates are used due to rotation symmetry. The origin is at the nozzle exit of the printhead and the x-Axis is the direction of the free jet.  $r$  is the radial direction and  $\phi$  the azimuthal angle. In order to determine the position of the focal point, the particle tracks from the CFD are exported. These records feature the position of each particle throughout all simulated timesteps. The resulting dataset can then be scanned through step by step and the  $r$ -position of each particle can be calculated. Because there are a thousand particles distributed in all azimuthal angles and due to rotational symmetry of the geometry it is assumed that the coordinate  $\phi$  is of no relevance to the jet and that it is sufficiently round along its entire travel distance. Therefore, determining the radial distance  $r$  to the center axis is sufficient to determine the size of the aerosol jet.

While scanning through the dataset the size of the aerosol jet in each cross section is imposed by the particle that is furthest away from the x-Axis. Stray particles cause overspray on the substrate which leads to undefined boundaries in the print image and can have serious effects on the function. Therefore it is important to consider outliers when determining where the focal point lies. When the focal point is found it can be described by its x-position  $x_{Focal}$ , which will be called the focal point position throughout this paper, and the  $r$ -position of the most outward particle in the focal plane  $r_{Focal}$  which is called the Focal Spot Half Width (FSHW) throughout this paper.

### 3.3 Automatic Parameterization

As the atomizer unit is what sets the AoD printing method apart from other technologies, as mentioned in Section 1, its development is of great importance. While the sheath gas in combination with the nozzle geometry has the biggest influence on the focusing of the aerosol spray, its flow is assumed to be stationary under operating conditions. The biggest remaining influence on the position of the focal point of the aerosol spray lies in the atomization of the ink and what the initial attributes of the individual droplets are when they enter the mixing chamber. Relevant attributes are the mass and direction of travel of a particle. Therefore, a study of what values are advantageous is highly desirable as it can be used to guide further development of the atomization unit.

For this purpose, a parametric study of the parti-

cle's mass  $m$  and angle of injection  $\theta$  is made. The injection angle was chosen as it describes the direction of travel of the particles in the *cone injection* model of Ansys Fluent. More detail about the definition of the *cone injection* model can be found in ANSYS, Inc. (2023b). The decision is made to incorporate Kadi4Mat v0.45.3 (Brandt et al., 2021), an electronic lab notebook (ELN), into the process in order to easily store data in a uniform and code accessible way. The boundaries for the parametric study are taken from previous studies (Ungerer et al., 2023a). The particle size and therefore mass is varied from  $1.05 \times 10^{-5}$  m to  $1.85 \times 10^{-5}$  m radius with a step size of  $0.05 \times 10^{-5}$  m. The injected droplets are set to be liquid water at a temperature of 300 K and since there is no active heating or cooling present, the density of the water doesn't change significantly and the droplet size correlates directly with the droplet mass. The injection angle  $\theta$  is varied from  $0^\circ$  to  $45^\circ$  in  $5^\circ$  steps. The result is a set of 17 simulations with varying mass at a constant injection angle of  $35^\circ$  and a second set of ten simulations with a varying injection angle at a constant mass of 1.2859 ng which results from a particle radius of  $1.35 \times 10^{-5}$  m.

Fluent allows for the continuation of previously simulated cases. Because the aerosol is simulated through a Lagrange-Euler model it doesn't affect the flow of the continuous phases. This allows the simulation of one case until the sheath gas flow has fully developed. Once convergence is reached in that case it is saved as a base case. In order to save on computation time all simulations will use the fully developed flow from the base case as a starting point by loading the case data from the base case, modifying the injection parameters and continuing the simulation. Due to the different injection parameters the residuals will spike and the simulation is run until they are back below the boundaries for convergence.

Each simulation gets its own record in Kadi4Mat which features all of the data that differs from the base case which is linked in the record as well. A script is written in Python 3.11.3 which loads the base case into Fluent via the Kadi\_apu v.0.35.0 and ansys-fluent-core v.0.18.2 Libraries. Afterwards the code modifies the relevant parameters specified in the ELN records and starts the simulation with the modified parameters. After the simulation has finished, the Python code saves the finished simulation data back into its corresponding record where it can be accessed for evaluation.

For the evaluation MATLAB 2023b is used. As the influence of the initial condition on the focal point of the individual particle is of interest, the focal point needs to be evaluated for each individual particle as

well. The method is equivalent to the method described in Section 3.2. The result is a set of 1000 focal points with their corresponding initial conditions.

The relationship between the initial conditions and the focal point is complex. In order to gain simplified correlations a model reduction is attempted through the parametric study and a mathematical model needs to be selected. For this example, it is assumed that the mass and injection angle do not affect each other and that their influences on the focal point are independent. They can then be separated mathematically into the individual influence functions  $F_{pq}$  which describes the influence that the variable  $q$  has on the variable  $p$ . These functions are determined by examining the change of the focal point position and FSHW throughout the simulations where the initial conditions  $m$  and  $\theta$  of the particles are modified. In each of the previously mentioned two sets of simulations only one initial condition is modified while the other remains the same. By plotting the focal point position and FSHW over the initial condition their relation can be displayed. The influence functions  $F_{pq}$  are determined by fitting a regression curve to the results.

Because each influence function describes the absolute position and half width of the focal point adding them together results in the doubling of both values. In order to negate that effect a fixed offset value is added to the influence function. Equations 2 and 3 show the final equations to determine the focal point position and FSHW of a particle based on its initial conditions in a fully developed sheath gas flow.

$$x_{Focal}(m, \theta) = F_{xm}(m) + F_{x\theta}(\theta) + x_{offset} \quad (2)$$

$$r_{Focal}(m, \theta) = F_{rm}(m) + F_{r\theta}(\theta) + r_{offset} \quad (3)$$

## 4 PARAMETRIC STUDY

### 4.1 Determining the Focal Point

When exporting the particle tracks, every particle is listed with all of its positions and mass at every timestep it is simulated. Naturally not all particles share the same x-coordinate in the same row of the export file. Therefor the MATLAB code scans the file row by row and looks for previously specified x-positions of a particle. If the specified x-position lies between two x-positions from the exported file, all variables are interpolated linearly. The result is a dataset with synchronized data of all particles at specific cross sections. The cross sections were evaluated in intervals of 0.1 mm starting at the nozzle exit. For

each cross section the r-position and mass of each particle is saved in a text file.

In a second step all of the cross sections can be evaluated as described in Section 3.2. The result is displayed in Figure 6 where the half width of the aerosol jet is plotted over the distance from the nozzle exit. The focal point is marked as well.

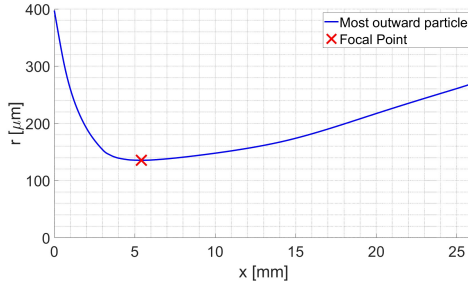


Figure 6: Half width of the aerosol jet after exiting the nozzle.

The accuracy of the focal point depends on the distance between slices that are evaluated. The plotted values in Figure 6 belong to a simulation with a Rosin-Rammler mass distribution and a random injection angle up to  $45^\circ$  for each particle. The simulation will be discussed later in more detail.

## 4.2 Model Reduction

As described in Section 3.3 a parametric study with varying mass and injection angle is simulated to determine whether these have a significant influence on the focal point. The initial parameters in the simulations are tightly controlled and random variance is suppressed. The focal point position of each individual particle, i.e. the point of each individual particle with the closest distance to the central axis, as well as the FSHW can be determined in an analogue way as the entire jet. After determining these parameters for each particle in one simulation, the median, minimum and maximum values are determined and plotted over the varied parameter. For the mass variance these graphs are shown in Figure 7.

The solid line represents the median and the dashed lines the minimum and maximum value respectively. The small span of the data for each mass indicates that the influence of the particle mass dominates the position and half width of the focal point if the injection angle is kept constant. In addition, the graph shows a linear effect of particle mass on the focal point position with a more massive particle increasing the x-position, which is desirable. The effect of the particle mass on the FSHW seems quadratic within the observed boundaries. A more massive par-

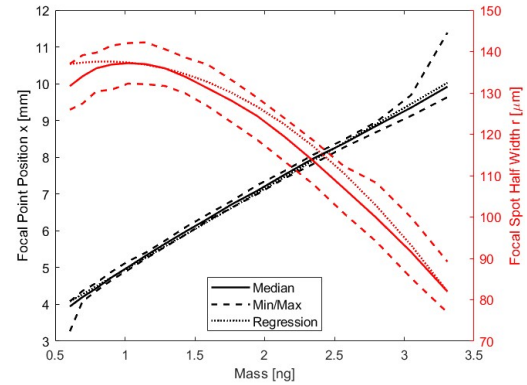


Figure 7: The influence of the particle mass on the focal point position and FSHW.

ticle also resulting in a smaller half width is also desirable. For both curves their respective regression functions were determined to:

$$F_{xm}(m) = 2.1996 \times 10^{12} \frac{\text{mm}}{\text{kg}} \cdot m + 2.747 \text{ mm} \quad (4)$$

$$F_{rm}(m) = -9.2749 \times 10^{21} \frac{\text{mm}}{\text{kg}^2} \cdot m^2 + 1.597 \times 10^{10} \frac{\text{mm}}{\text{kg}} \cdot m + 0.1288 \text{ mm} \quad (5)$$

The regression functions are plotted in Figure 7 as the dotted line. The coefficient of determination for the regression curves are  $R_{xm}^2 = 99.6\%$  and  $R_{rm}^2 = 97.7\%$

For the influence of the injection angle the graph shows a similarly small span of the datasets. As can be seen in Figure 8 the injection angle has no effect on the focal point position. The zero-degree simulation is a special case which represents an injection where all particles are injected in a line oriented along the x-axis. Naturally, this results in a much smaller size and it moves the focal point very close to the nozzle exit as the particle tracks will widen in the free jet due to turbulence effects. Hence, the influence of the zero-degree simulation is neglected for determining the focal point position.

The influence of the injection angles on the FSHW seems to follow an exponential curve. For simplicity and linearity, the regression fit was made with a quadratic function. The resulting regression functions are:

$$F_{x\theta}(\theta) = 0 \quad (6)$$

$$F_{r\theta}(\theta) = -3.915 \times 10^{-5} \frac{\text{mm}}{\text{o}^2} \cdot \theta^2 + 3.9603 \times 10^{-3} \frac{\text{mm}}{\text{o}} \cdot \theta + 4.5856 \times 10^{-2} \text{ mm} \quad (7)$$

The corresponding coefficient of determination is  $R_{r\theta}^2 = 99.3\%$ . Each of the influence functions besides

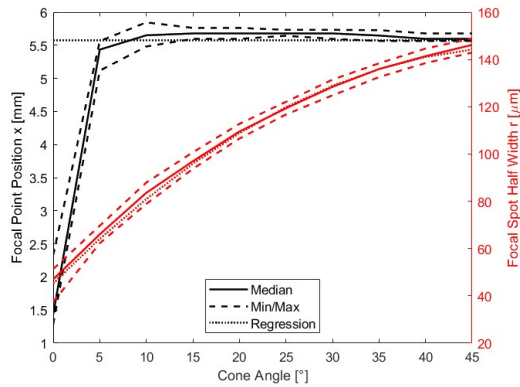


Figure 8: The influence of the injection angle on the focal point position and FSHW.

$F_{x\theta}$  describes the absolute value of the position or half width of the focal point. As the individual influence equations are added together according to Equations 2 and 3 the results are too large as the absolute position and half width is evaluated twice. An offset is necessary to correct the functions. Since  $F_{x\theta} = 0$  there is no need for an offset to the x-Position and  $F_{xm}$  fully describes the focal point position. For the FSHW the point:

$$r_{Focal}(1.2859 \text{ ng}, 35^\circ) = 135.94 \mu\text{m} \quad (8)$$

is chosen as a boundary condition as the two sets of simulation share one simulation with these initial parameters.  $r_{offset}$  is determined through the boundary condition and the resulting functions for  $x_{Focal}$  and  $r_{Focal}$  are:

$$x_{Focal}(m) = F_{xm}(m) \quad (9)$$

$$r_{Focal}(m, \theta) = F_{rm}(m) + F_{r\theta}(\theta) - 0.13457 \text{ mm} \quad (10)$$

### 4.3 Validation of the Reduced Model

As the testbed at our institute is currently inoperable, a theoretical approach for validation is chosen. In order to validate the determined influence functions a simulation using a random distribution for the particle parameters is simulated. The injection angle  $\theta$  is randomized by using a solid cone as the injection model (Ungerer et al., 2023d). The size, and hence the mass of the droplets, has previously been measured by Walter (2022) and the results are shown in Figure 9. In order to emulate the measurements in the simulation environment, a distribution curve is fitted to the results. A commonly used distribution for particle size is the Rosin-Rammler distribution (ANSYS, Inc., 2023b). The distribution revolves around a mean diameter  $\bar{d}$  of the droplets and a spread parameter  $N_r$  in order to calculate the mass fraction  $Y_d$  of all

droplets that have a diameter greater than  $d$ :

$$Y_d = e^{-(d/\bar{d})^{N_r}} \quad (11)$$

Ansys Fluent offers the distribution by assigning each particle one of several distinct sizes. The user can enter the minimum, maximum and mean size, spread parameter  $N_r$  as well as how many distinct sizes Ansys should define. The displayed droplet sizes match the boundaries introduced in Section 3.3 and therefore result in the same masses as examined throughout this paper spanning approximately 0.6 ng to 3.3 ng. The resulting inputs for Fluent are listed in Table 1. The number of diameters determines how many evenly spaced, discrete masses Fluent can assign to the particles. Ten was chosen to reflect the ten measured intervals from Figure 9.

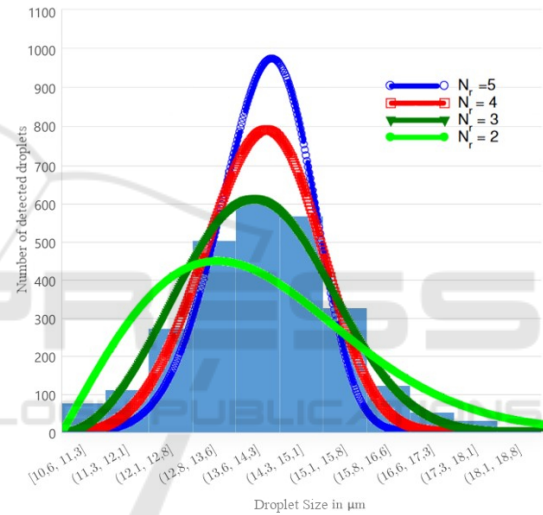


Figure 9: Histogram of measured droplet sizes with various Rosin-Rammler distributions (Walter, 2022).

Table 1: The Rosin-Rammler Size Distribution values.

Minimum Radius	10.5 $\mu\text{m}$
Mean Radius	13.9 $\mu\text{m}$
Maximum Radius	18.5 $\mu\text{m}$
Spread Parameter $N_r$	3
Number of Diameters	10

The mass of each particle can be read from the export of the particle tracks. The injection angle of each particle is determined by observing the cross section of the aerosol 0.1 mm away from the capillary. It is assumed that the sheath gas has no major influence on the position of the particles near their injection point. The injection angle for each particle is then calculated by taking the arctangent:

$$\theta = \text{atan}\left(\frac{r_{0.1 \text{ mm}}}{0.1 \text{ mm}}\right) \quad (12)$$

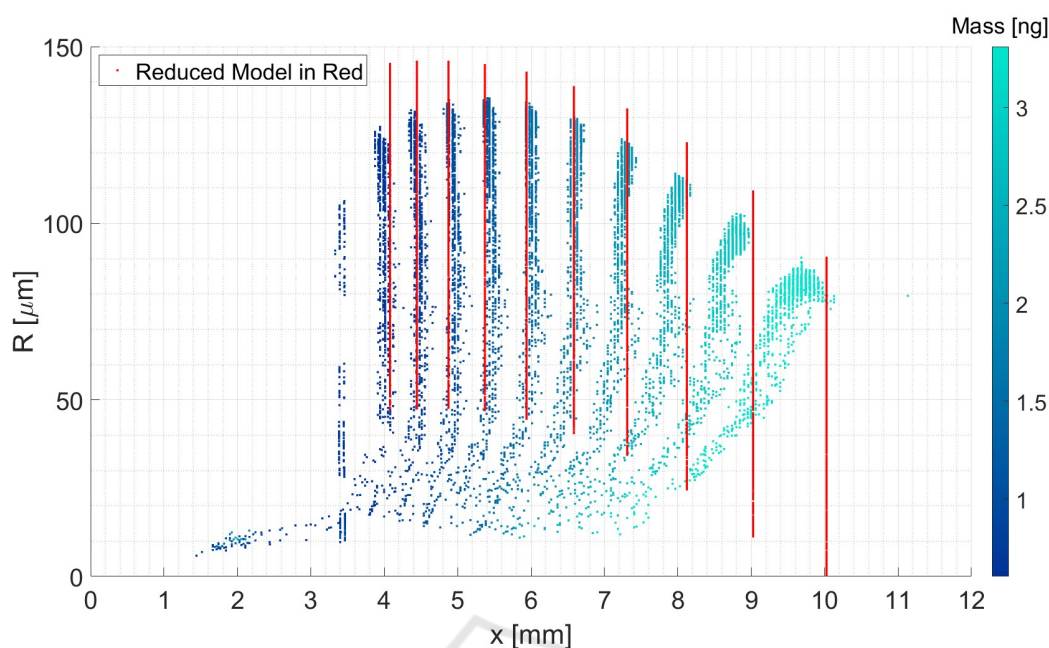


Figure 10: The focal point position and half width of each particle from the Rosin-Rammler simulation as well as from the reduced model. The focal points belonging to the Rosin-Rammler simulation are colored by the particle mass. The estimated focal points by the reduced model are displayed in red.

Using the initial conditions  $m$  and  $\theta$  and Equations 9 and 10 the assumed focal point position and FSHW for each particle is calculated. The actual position and half width of the focal points is determined as described in Section 3.3.

Figure 10 shows the calculated focal point positions (shown in red) and those simulated with the Rosin-Rammler distribution (colored by the particle mass). The focal points are sorted into ten easily distinguishable groups depending on their mass. For bigger masses, the focal point position increases. For particle masses smaller than 2.5 ng there is good agreement between the prediction and the simulation.

Looking at the injection angles, it can also be observed that particles with a larger injection angle have a larger focal length. The corresponding graph can be found in the Appendix.

## 5 RESULTS AND DISCUSSION

The results of the Rosin-Rammler simulation which are shown in Figure 10 make it apparent that there are effects that have not been captured by the reduced model. The results from Section 4.2 predict that the injection angle has no effect on the focal point position. This is largely true for the groups of particles with a lower mass. Their columns on the left side in Figure 10 are mostly vertical whereas the columns of

particles with more mass to the right are slanted. This means that for particles with a higher mass, the injection angle starts affecting the Focal Point Position or a third, not previously evaluated, effect plays a role. This has not been captured by the parametric study. In order to combat this discrepancy, more parameter combinations can be simulated. If computing time is of concern the main simulations to determine a model can be handled as shown in this paper. But in addition, random sample simulations can be scattered through the boundaries of the initial parameters to validate the determined model. The effect that for more massive particles the injection angle gains influence on the focal point position could have been observed in this case and the independent model reduction could have been discarded or extended sooner.

As no reduced model is perfect there is a need to determine a validity domain. The validation criteria depend on the context but for this example an allowed relative error of the reduced model compared to the Rosin-Rammler simulation is chosen. For the focal point position a relative error of 5% in either direction is considered acceptable. For the FSHW a relative error of 5% was deemed acceptable if the reduced model predicts a larger half width. But as overspray is an issue for the AoD printing process, no error is tolerated if the reduced model predicts a smaller half width than the resulting simulation. The relative errors in both dimensions are calculated for all particles



and plotted over their initial parameters. The plots can be seen in Figures 11 and 12.

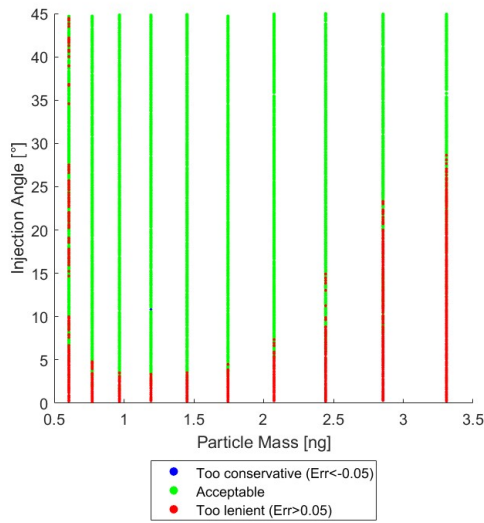


Figure 11: The relative error of the focal point position when comparing the reduced model to the Rosin-Rammler simulation colored by acceptance.

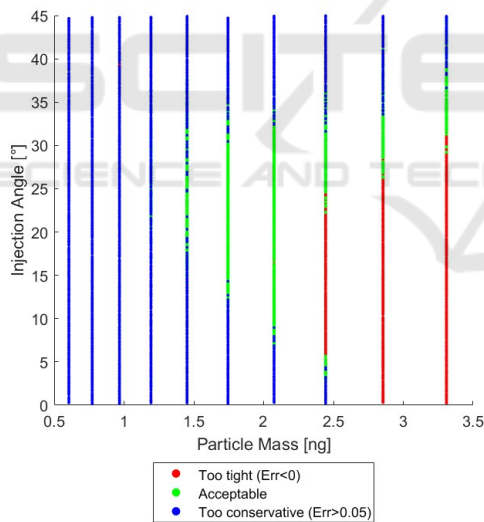


Figure 12: The relative error of the FSHW when comparing the reduced model to the Rosin-Rammler simulation colored by acceptance.

The focal point position is described well for larger injection angles. Towards  $0^\circ$  the deviation becomes too large as the focal point shifts closer to the nozzle as described earlier in this section. The FSHW has a low validity domain under the selected tolerances. For most initial conditions the estimate by the reduced model is too conservative and the FSHW is predicted too big. This is not necessarily harmful for

the AoD process as the aerosol jet will be smaller than the reduced model describes. However, the error quickly becomes too large. Additionally, towards the more massive particles the estimate becomes too tight. This likely results out of the dependence of the two initial parameters which is not considered by the reduced model yet seen by the slantedness of the more massive particle groups in Figure 10. The result is that the two influence functions  $F_{rm}$  and  $F_{r\theta}$  both go towards a negative direction when approaching big masses and small injection angles respectively. These two influences added together even result in negative FSHWs at the extreme cases. Clearly the reduced model offers only limited validity around 1.85 ng and  $22^\circ$  for determining the FSHW.

From this point there are multiple options: Boundaries in which the reduced model is limited can be determined and saved in an ELN. If any future simulations fall into those boundaries the reduced model can be taken advantage of in order to reduce computation time in the future. If the reduced model is not deemed accurate enough a different mathematical model can be assumed and evaluated in order to determine the best model reduction. Additionally, the reduced model can be discarded but the general trends can be used. In this example it was discovered that bigger particles and smaller injection angles are favorable to reduce the FSHW in the free jet. This information can be kept in mind when developing the atomizer unit. What path is the most sensible depends on the application that this method is adapted to.

## 6 CONCLUSIONS AND OUTLOOK

A method for an automated parametric study through the example of an AoD jet-printhead has been debated in this paper. The method contains an organized data storage through the use of the ELN Kadi4Mat. All steps described in Sections 3 and 4 of this paper can be done by scripts and application programming interfaces (APIs) of relevant software.

The method has been applied successfully to have the computer semi-autonomously determine a reduced model of a flow phenomena. While the model reduction made in this paper did not prove accurate enough to describe the focal point of a particle loaded stationary flow outside of a specified domain, that was not the main intention of this paper. It was merely a simple example of the proposed method in action. In a greater context than this paper would support, more sophisticated models can be used as a basis for the model reduction and comparisons between differ-

ent models could be made to determine the best. If paired with physical tests, model parameters can be changed in the CFD software and the resulting flow can be compared to real observation in order to determine which model parameters reflect reality the best. This possibility is the basis of a digital twin that is currently being developed at KIT. The digital twin is supposed to accompany the AoD printing procedure featured in this paper. The AoD printhead represents a complex problem with many interactions that are not sufficiently describable by established theories. The method presented in this paper can help to develop empirical models in a semi-automated way. While human supervision is still necessary, the workload is greatly reduced. Another possibility is that a human can root the automatically generated empirical models through established theory and push the understanding of the corresponding field forwards.

Another possibility for this method is the model reduction. Only one simple type of mathematical model has been examined in this paper. However, it is possible to try several different mathematical model reductions of complex problems and see which reduction does the best at emulating the complex interaction. This would result in computationally cheaper correlations which lessens the calculational load of a digital twin.

The main advantage of this method is the adaptability. The ELN provides a good structure for orderly and automated data storage. As long as the simulation software of interest supports scripted processes through an API, the procedure can be adapted. The setup of this method is labor-intensive based on the scope of what it is adapted to as all options for parametrization need to be coded in. This effort is also heavily dependent on the quality and flexibility of the API of the simulation program. This makes it suitable for larger or long-term applications such as a digital twin where the overhead cost of programming is smaller compared to the work that is saved throughout the lifespan of the model.

## ACKNOWLEDGEMENTS

The mesh independence study as well as the determining of the Rosin Rammler distribution values were done by Tim Walter who we thank for his contributions.

The authors confirm that no artificial intelligence (AI) was used in generating the text of this article.

## REFERENCES

- ANSYS, Inc. (2023a). *Ansys Fluent Theory Guide*. ANSYS, Inc., release 2023 r1 edition.
- ANSYS, Inc. (2023b). *Ansys Fluent User's Guide*. ANSYS, Inc., release 2023 r1 edition.
- Baby, T. T., Marques, G. C., Neuper, F., Singaraju, S. A., Garlapati, S., von Seggern, F., Kruk, R., Dasgupta, S., Sykora, B., Breitung, B., Sukkurji, P. A., Bog, U., Kumar, R., Fuchs, H., Reinheimer, T., Mikolajek, M., Binder, J. R., Hirtz, M., Ungerer, M., Koker, L., Gengenbach, U., Mishra, N., Gruber, P., Tahoori, M., Hagemann, J. A., von Seggern, H., and Hahn, H. (2020). Printing technologies for integration of electronic devices and sensors. In Sidorenko, A. and Hahn, H., editors, *Functional Nanostructures and Sensors for CBRN Defence and Environmental Safety and Security*, NATO Science for Peace and Security Series C: Environmental Security, pages 1–34. Springer Netherlands, Dordrecht.
- Brandt, N., Griem, L., Herrmann, C., Schoof, E., Tosato, G., Zhao, Y., Zschumme, P., and Selzer, M. (2021). Kadi4mat: A research data infrastructure for materials science. *Data Science Journal*, 20:8. <https://datascience.codata.org/articles/10.5334/dsj-2021-008>.
- Choi, H. W., Zhou, T., Singh, M., and Jabbour, G. E. (2015). Recent developments and directions in printed nanomaterials. *Nanoscale*, 7(8):3338–3355.
- Cui, Z., editor (2016). *Printed electronics: Materials, technologies and applications*. John Wiley & Sons, Higher Education Press, Singapore, 1st edition.
- Gengenbach, U., Ungerer, M., Aytac, E., Koker, L., Reichert, K.-M., Stiller, P., and Hagenmeyer, V. (2018). An integrated workflow to automatically fabricate flexible electronics by functional printing and smt component mounting. In Vogel-Heuser, B. and Lennartson, B., editors, *Proc. 14th IEEE International Conference on Automation Science and Engineering (CASE)*, pages 1624–1629.
- IDS Inc. (2024). Nanojet aerosol print technology. <https://www.idsnm.com/>. Last accessed on Feb. 12, 2024.
- IDTechEx Ltd. (2022). 3d electronics/additive electronics 2022-2032: 3d printed electronics, molded interconnect devices, in-mold electronics, aerosol jet, 3d metallization, laser direct structuring, additively manufactured electronics. sample pages. <https://www.idtechex.com/en/research-report/3d-electronics-additive-electronics-2022-2032/860>. Last accessed on Feb. 12, 2024.
- Magdassi, S., editor (2010). *The chemistry of inkjet inks*. World Scientific Publishing, Singapore.
- Menter, F. R. (1994). Two-equation eddy-cisosity turbulence models for engineering applications. *AIAA Journal*, 32(8):1598–1605.
- Optomec Inc. (2024). Aerosol jet technology. <https://optomec.com/printed-electronics/aerosol-jet-technology/>. Last accessed on Feb. 12, 2024.
- Sieber, I., Thelen, R., and Gengenbach, U. (2020a). Assessment of high-resolution 3d printed optics for the use case of rotation optics. *Optics express*, 28(9):13423–13431.
- Sieber, I., Thelen, R., and Gengenbach, U. (2020b). Enhancement of high-resolution 3d inkjet-printing of op-

tical freeform surfaces using digital twins. *Micromachines*, 12(1).

- Sieber, I., Zeltner, D., Ungerer, M., Wenka, A., Walter, T., and Gengenbach, U. (2022). Design and experimental setup of a new concept of an aerosol-on-demand print head. *Aerosol Science and Technology*, pages 1–12.
- Sirringhaus, H. and Shimoda, T. (2003). Inkjet printing of functional materials. *MRS Bulletin*, 28(11):802–806.
- Suganuma, K. (2014). *Introduction to printed electronics*, volume 74 of *SpringerBriefs in Electrical and Computer Engineering*. Springer Science+Business Media, New York and Heidelberg and Dordrecht and London, 1st edition.
- Ungerer, M. (2020). *Neue Methodik zur Optimierung von Druckverfahren für die Herstellung funktionaler Mikrostrukturen und hybrider elektronischer Schaltungen: [New methodology for the optimization of printing processes for the fabrication of functional microstructures and hybrid printed electronics]*. Dissertation, Karlsruhe Institute of Technology, Karlsruhe.
- Ungerer, M., Benítez, J. L., Zeltner, D., Wenka, A., Gengenbach, U., and Sieber, I. (2023a). Modelling and design-for-manufacturing of an aerosol-on-demand jet-printhead. In Wagner, G., Werner, F., and de Rango, F., editors, *Simulation and Modeling Methodologies, Technologies and Applications*, volume 780 of *Lecture Notes in Networks and Systems*, pages 1–21. Springer International Publishing, Cham.
- Ungerer, M., Gengenbach, U., Grewal, K. S., Wenka, A., and Sieber, I. (5/28/2023 - 5/31/2023b). Design-for-manufacture of a dual-chamber nozzle for hydrodynamic focusing of the aerosol-on-demand jet-printhead. In *2023 Symposium on Design, Test, Integration & Packaging of MEMS/MOEMS (DTIP)*, pages 1–5. IEEE.
- Ungerer, M., Hofmann, A., Scharnowell, R., Gengenbach, U., Sieber, I., and Wenka, A. (2023c). Print head and printing method - tête d'impression et procédé d'impression.
- Ungerer, M., Walter, T., and Sieber, I. (2023d). Position analysis of the atomiser unit of an aerosol-on-demand jet-printhead by means of computational fluid dynamics. In *Proceedings of the 13th International Conference on Simulation and Modeling Methodologies, Technologies and Applications*, pages 126–133. SCITEPRESS - Science and Technology Publications.
- Ungerer, M., Zeltner, D., Wenka, A., Gengenbach, U., and Sieber, I. (2022). Modelling and simulation of an aerosol-on-demand print head with computational fluid dynamics. In *Proceedings of the 12th International Conference on Simulation and Modeling Methodologies, Technologies and Applications*, pages 44–51. SCITEPRESS - Science and Technology Publications.
- Walter, T. (2022). Modellvalidierung eines aerosol-on-demand jet-druckkopfes auf basis experimenteller sowie simulativer analysen und anpassungen.
- Wilcox, D. C. (2006). *Turbulence Modeling for CFD*. DCW Industries Inc., 3rd edition.

## APPENDIX

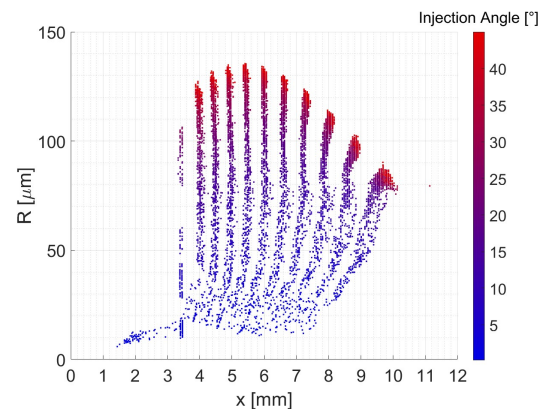


Figure 13: Figure 10 with the particles colored by their Injection Angle  $\theta$ .